

RESEARCH ARTICLE

10.1002/2014JG002774

Key Points:

- A new method for estimating leaf area from multireturn lidar in complex forest
- Simulation data sets to test the inversion algorithm
- A case study of a moist tropical forest

Supporting Information:

- Data Set S1

Correspondence to:

M. Detto,
dettom@si.edu

Citation:

Detto, M., G. P. Asner, H. C. Muller-Landau, and O. Sonnentag (2015), Spatial variability in tropical forest leaf area density from multireturn lidar and modeling, *J. Geophys. Res. Biogeosci.*, 120, doi:10.1002/2014JG002774.

Received 21 AUG 2014

Accepted 25 JAN 2015

Accepted article online 30 JAN 2015

Spatial variability in tropical forest leaf area density from multireturn lidar and modeling

Matteo Detto¹, Gregory P. Asner², Helene C. Muller-Landau¹, and Oliver Sonnentag³

¹Smithsonian Tropical Research Institute, Panama City, Panama, ²Carnegie Institution for Science, Palo Alto, California, USA, ³Département de géographie, Université de Montréal, Montréal, Quebec, Canada

Abstract Leaf area index and leaf area density profiles are key variables for upscaling from leaves to ecosystems yet are difficult to measure well in dense and tall forest canopies. We present a new model to estimate leaf area density profiles from discrete multireturn data derived by airborne waveform light detection and ranging (lidar), a model based on stochastic radiative transfer theory. We tested the method on simulated ray tracing data for highly clumped forest canopies, both vertically homogenous and vertically inhomogeneous. Our method was able to reproduce simulated vertical foliage profiles with small errors and predictable biases in dense canopies (leaf area index = 6) including layers below densely foliated upper canopies. As a case study, we then applied the method to real multireturn airborne lidar data for a 50 ha plot of moist tropical forest on Barro Colorado Island, Panama. The method is suitable for estimating foliage profiles in a complex tropical forest, which opens new avenues for analyses of spatial and temporal variations in foliage distributions.

1. Introduction

Leaf area density, the leaf area per unit of volume, is one of the most important ecophysiological attributes of vegetation, as it is a key variable for upscaling many processes from leaves to ecosystems [Jarvis and McNaughton, 1986]. Not only does foliage intercept radiation, transpire, and photosynthesize, and exchanges other various gases, it also intercepts precipitation and is subject to deposition of atmospheric aerosols. Despite its importance, leaf area density and its three-dimensional (3-D) variation in space over large areas remains challenging to estimate, especially in natural forest ecosystems [Bréda, 2003].

The three-dimensional distribution of foliage in forests is influenced by multiple factors expressed at different spatial and temporal scales. Within a plant, leaves are clustered along twigs, branches, and stems. At the stand level, the within-crown foliage distribution is determined by competition for light and other resources and also by the type and frequency of disturbances (e.g., canopy gaps) and successional trajectories. At the landscape level, heterogeneity in soil, climate, and disturbances such as fires, landslides, and windthrows contributes to large-scale variability in tree and thus foliage distributions. As a result, the structure of forests, such as those found throughout the humid tropics, is famously structurally complex. A single hectare of tropical forest, for example, may contain hundreds of species of different life forms including shrubs, trees, lianas, and epiphytes; thus, it is a particularly difficult challenge to understand how these plants, and their foliage, fill space in three dimensions.

This structural complexity and associated spatial variation in leaf area density has important consequences for ecosystem functions and dynamics [Shugart *et al.*, 2010]. For example, simulations of light interception and energy fluxes are strongly affected by the vertical profile of leaf area, even if the total amount of leaves in the canopy remains the same [Wu *et al.*, 2000]. Because of the difficulty of directly measuring such distributions (for tropical forests in particular, there is to our knowledge only one study that has ever directly measured landscape leaf area index by harvesting vegetation in multiple vertical profiles [Clark *et al.*, 2008]), indirect methods have been developed to estimate leaf area index from optical instruments [Chen *et al.*, 1997] and satellite-derived vegetation indices. However, these methods tend to systematically underestimate leaf area index and have important shortcomings for assessing spatial variability [Olivas *et al.*, 2013]. For example, passive remote sensors often suffer from signal saturation [Gamon *et al.*, 1995], which limits insights into both vertical and horizontal spatial variabilities. The ground-level measurements tend to underestimate leaf area in the upper canopy [Parker *et al.*, 2004; Hosoi *et al.*, 2013] and require knowledge of leaf clumping. However, small detectable differences in radiation measurements may correspond to larger differences in leaf area.

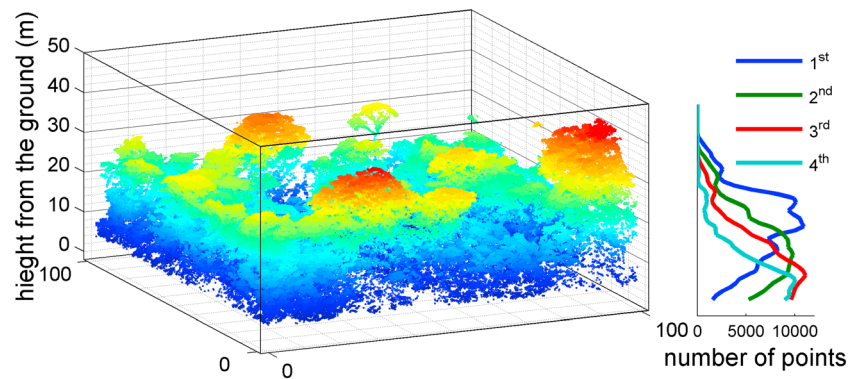


Figure 1. Example of a forest point cloud obtained using an airborne discrete-return lidar above a hectare of tropical forest on Barro Colorado Island. Colors indicate height (m). The vertical distribution of points by return number is also shown for reference.

Airborne waveform light detection and ranging (lidar) systems provide important advantages for capturing forest structural complexities in 3-D [Asner *et al.*, 2012a, 2012b], as lidar records the entire backscattered signal of each emitted laser pulse [Wagner *et al.*, 2004]. Waveform lidar data are often decomposed into their components of echoes characterizing different targets along the path of the laser beam [Wagner *et al.*, 2007], thereby producing discrete-return data (e.g., Figure 1). First returns originate from the first objects that a laser pulse encounters, often the upper part of a vegetation canopy. In contrast, second and later returns originate from the portion of a pulse passing through gaps or being transmitted by leaf tissues into lower vegetation layers, eventually reaching the ground surface. The penetration capability of waveform lidar can thus overcome the problem of signal saturation and clumping, enabling a better characterization of spatial and temporal variability of foliage distribution.

Lidar has been used in a wide range of applications related to forest ecology [Lefsky *et al.*, 2002], including (but not limited to) estimation of aboveground carbon stocks [Asner *et al.*, 2010] and their spatial and temporal variation [Mascaro *et al.*, 2011; Detto *et al.*, 2013; Meyer *et al.*, 2013], characterization of animal habitats, and quantification of landscape fragmentation [Flaspohler *et al.*, 2010; McMahon *et al.*, 2015].

We can heuristically interpret the laser point cloud derived from a small-footprint (< 3 m resolution) lidar as a set of points obtained by penetrating the forest canopy with a needle-like beam. Each point associated with the k th return is the intersection between the canopy element and the penetrating beam at the k th contact. This simple idealization does not consider the intensity of the return and focuses solely on three factors: foliage spatial arrangement including (i) leaf orientation and (ii) clumping and (iii) laser scan angle. The needle analogy suggests that the lidar point cloud be analyzed as a stochastic point process [Daley and Vere-Jones, 2003].

Several methods have been developed to relate statistical properties of the lidar point clouds with statistical properties of the underlying vegetation. These include empirical (phenomenological) approaches [Richardson *et al.*, 2009; Zhao and Popescu, 2009; Hardiman *et al.*, 2011; Stark *et al.*, 2012] as well as physically based approaches such as ray tracing models and analytical or semianalytical radiative transfer models [Ni-Meister *et al.*, 2001; Kotchenova, 2003; Béland *et al.*, 2014], the latter being the focus of this study. The equations for radiative transfer in a stochastic medium were presented by Titov [1990] for scattered clouds and then applied to discontinuous canopies by Shabanov *et al.* [2000]. In their approach, foliage is represented by a spatial stochastic function with known statistical properties, in particular the first and second moments, which describe the foliar vertical profile and clumping, respectively.

Here we develop a modified version of the radiative transfer model described by Titov [1990] and Shabanov *et al.* [2000] for small-footprint, multireturn lidar data that enable estimation of leaf area index (LAI) and leaf area density (LAD), and its variation in 3-D space. We first apply this model to simulated data sets to evaluate its precision and accuracy (errors and biases) under ideal conditions as a function of canopy complexity, pulse, and return numbers. Then, we apply this model to an empirical case study of airborne lidar data for a moist tropical forest, thus demonstrating its ability to estimate vertical and horizontal variability in LAD.

2. Methods and Data

2.1. Theory: Stochastic Radiative Transfer Model

We represent foliage spatial arrangement as a stochastic process described by the indicator function $p(\mathbf{x})$, which is equal to 1 if there is a leaf in a volume element including $\mathbf{x}(x,y,z)$ and 0 otherwise. Each foliated point is characterized by a leaf area volume density a_L , defined as the expectation of the one-sided leaf area per unit volume with leaves, and a leaf inclination angle, defined as the angle between the leaf surface normal and the zenith [Ross, 1981]. Assuming horizontal homogeneity, the leaf area density, $u(z)$, at any depth z into the canopy is defined as

$$u(z) = a_L P_z [p(x, y, z) = 1] = a_L E_z [p] \quad (1a)$$

where $P_z[\cdot]$ and $E_z[\cdot]$ are probability and expectation taken over a horizontal plane at depth z ($z=0$ corresponds with the top of the canopy). Similarly, the effective leaf area density, $u_E(z, \vec{\Omega})$, the projection of foliage area in a unit of volume in the beam direction $\vec{\Omega} = (\Omega_x, \Omega_y, \Omega_z)$, is defined as

$$u_E(z, \vec{\Omega}) = G(z, \vec{\Omega}) u(z) \quad (1b)$$

where $G(z, \vec{\Omega})$ is the estimated projection function of the leaf area in the direction $\vec{\Omega}$ per unit leaf volume, which depends on the leaf inclination angle distribution function as defined in Ross [1981]. The spatial distribution of foliage is described by the pair correlation function $g(z, z', \vec{\Omega})$ which is the normalized expected value of the product of $p(\mathbf{x})$ taken at two planes z and z' in the direction of the beam $\vec{\Omega}$

$$g(z, z', \vec{\Omega}) = \frac{E_z \left[p(x, y, z) p \left(x + \frac{\Omega_x}{\Omega_z} z', y + \frac{\Omega_y}{\Omega_z} z', z' \right) \right]}{E_z [p] E_z [p]} \quad (2)$$

$g(z, z', \vec{\Omega})$ is equal to 1 if the leaves are randomly distributed (e.g., Poisson process) and generally > 1 for clumped distributions (e.g., negative binomial process).

The stochastic radiative transfer for uncollidional radiation, i.e., beams that do not interact with leaves, associated with the k th return ($k = 1, 2, \dots$), is well described by the a system of Volterra integral equations [Titov, 1990; Shabanov et al., 2000], modified to take the return number into account (Appendix A):

$$I(z, \vec{\Omega}, k) = I_0(\vec{\Omega}) - |\mu(\vec{\Omega})|^{-1} \int_0^z u(z') G(z', \vec{\Omega}) U(z', \vec{\Omega}, k) dz' \quad (3a)$$

$$\sum_{i=1}^k U(z, \vec{\Omega}, i) = U_0(\vec{\Omega}) - |\mu(\vec{\Omega})|^{-1} \int_0^z g(z, z', \vec{\Omega}) u(z') G(z', \vec{\Omega}) U(z', \vec{\Omega}, k) dz' \quad (3b)$$

where $I(z, \vec{\Omega}, k)$ is the mean radiation which penetrates to depth z in the direction $\vec{\Omega}$ associated with the k th return and $U(z, \vec{\Omega}, k)$ is the mean incident radiation intercepted by the canopy per unit of leaf area at depth z in the direction $\vec{\Omega}$ associated with the k th return; $|\mu(\vec{\Omega})|$ is the cosine of the polar angle in the direction $\vec{\Omega}$. To summarize, equations (3a) and (3b) say that the mean radiation and the mean radiation per unit of leaf area at any depth z equals the mean radiation at the top of the canopy, $I_0(\vec{\Omega})$ and $U_0(\vec{\Omega})$, respectively, minus a term which describes the mean radiation that has been intercepted between 0 and z .

2.2. Sampling by a Marked Point Process

Imagine the penetration of a forest canopy with beams and recording of the positions leaves are intersected. Each of these actions can be regarded as a realization of a marked point process defined by three random variables: ζ , ρ , and θ , indicating the vertical coordinates of the point, the sequential position along the beam (return number), and the beam inclination (scan angle), respectively. Given a statistically representative number of these realizations, the penetration functions at depth z_i , $l_{i,s,k}$ and $U_{i,s,k}$, associated with the k th return can be estimated from the following probabilities:

$$\frac{l_{i,s,k}}{l_{0,s}} = 1 - \frac{P(z < z_i, q = s, r = k)}{P(q = s, r = 1)} = 1 - \frac{\sum_{j=1}^i n_{j,s,k}}{\sum_{j=1}^m n_{j,s,1}} \quad (4a)$$

$$\frac{U_{i,s,k}}{U_{0,s}} = P(r = k | z_i - dz \leq z < z_i, q = s) = \frac{n_{i,s,k}}{\sum_{j=1}^{\infty} n_{j,s,k}} \quad (4b)$$

where $n_{i,s,k}$ is the number of points in the interval $(z_i - dz, z_i]$ with angle s and return number k .

The ratio $l_{i,s,k}/l_{0,s}$ can be interpreted as the probability for a beam with angle s to intercept fewer than k leaves up to depth z_i . For $k = 1$, $l_{i,s,1}/l_{0,s}$ is the proportion of beams which are not intercepted by leaves (gap fraction). The ratio $U_{i,s,k}/U_{0,s}$ can be interpreted as the probability for a leaf at depth z_i to be the k th contact along the beam path. For $k = 1$, $U_{i,s,1}/U_{0,s}$ equals the proportion of the leaf area which is directly exposed to radiation (sunlit leaves).

Because of laser beam attenuation, only points up to a maximum return number k_{\max} can be detected, and equation (4b) needs to be modified considering the following identity:

$$P(\rho = k | \rho \leq k_{\max}) = \frac{P(\rho = k)}{P(\rho \leq k_{\max})}.$$

Approximating equation (3b) with $g \approx 1$, a correction factor that takes into account a limited number of available returns can be applied to $U_{i,s,k}/U_{0,s}$ as

$$\frac{U_{i,s,k}}{U_{0,s}} \approx \frac{n_{i,s,k}}{\sum_{j=1}^{k_{\max}} n_{i,s,j}} \frac{l_{i,s,k_{\max}}}{l_{0,s}} \quad (5)$$

(see Appendix B for details).

2.3. Numerical Solutions

Solutions of equation (3a) are obtained by discretizing the system at regular intervals with step dz ($z_i, i = 1, 2, \dots, m$). A simple forward scheme provides the numerical solution of u_i for any given scan angle:

$$u_i = \frac{a_{i,s} - \sum_{j=1}^{i-1} u_j \beta_{j,s} dz}{\beta_{i,s} dz} \quad (6)$$

where

$$a_{i,s} = \frac{\sum_{j=1}^i n_{j,s,1}}{\sum_{j=1}^m n_{j,s,1}} \quad (7a)$$

$$b_{i,s} = \frac{G_{i,s}}{|\cos(s)|} \frac{n_{i,s,1}}{\sum_{k=1}^{k_{\max}} n_{i,s,k}} \left(1 - \frac{\sum_{j=1}^i n_{j,s,k_{\max}}}{\sum_{j=1}^m n_{j,s,k_{\max}}} \right) \quad (7b)$$

When the observations are taken at different scan angles, α and β can be computed as ensemble:

$$a_i = \frac{\sum_{s=0}^{90} \sum_{j=1}^i n_{j,s,1}}{\sum_{s=0}^{90} \sum_{j=1}^m n_{j,s,1}} \quad (8a)$$

$$b_i = \frac{\sum_{s=0}^{90} G_{i,s}}{\sum_{s=0}^{90} |\cos(s)|} \frac{n_{i,s,1}}{\sum_{k=1}^{k_{\max}} n_{i,s,k}} \left(1 - \frac{\sum_{j=1}^i n_{j,s,k_{\max}}}{\sum_{j=1}^m n_{j,s,k_{\max}}} \right) \frac{\sum_{j=1}^m n_{j,s,1}}{\sum_{s=0}^{90} \sum_{j=1}^m n_{j,s,1}} \quad (8b)$$

Commented MATLAB code to do these calculations is provided in Data Set 1 in the supporting information.

2.4. Simulated Data Sets and Their Analyses

We first tested the inversion algorithms on simulated data sets. To generate a strongly clustered distribution of geometrical elements, we used a family of point processes called the Shot Noise Cox Process (SNCP) [Møller, 2003], whose statistical properties are known (Appendix C). The SNCP can generate a large variety of clumped and inhomogeneous distributions. Its parameters can be loosely related to ecologically meaningful quantities (e.g., crown size, stem density, and dispersal distance; Table 1), and for this reason it is often used in spatial ecology [e.g., Henrys and Brown, 2009; Wiegand et al., 2009]. Because we are assuming horizontal homogeneity and isotropy in

Table 1. Model Parameters and Ecological Meaning for Simulated Datasets

| Parameter | μ | h | a, c | b, d | ℓ | r |
|--------------------------|--------------|-------------------|---|--|--------------------|---|
| Description | Stem density | Mean crown height | Allometric coefficients for crown size, density | Allometric exponents for crown size, density | Leaf size (length) | Vertical/horizontal crown anisotropic ratio |
| Vertically homogeneous | 4 | 15 ^a | 0.5, 1 | 0.0, 0.0 | 0.1 | 2 |
| Vertically inhomogeneous | 4 | 5 ^b | 0.5, 1 | 0.2, 2.0 | 0.1 | 2 |

^aUniform distribution.
^bExponential distribution.

azimuthal direction, we realize the point process in two dimensions only, for easy implementation and computational efficiency, over a horizontal distance of 200 m. At each point representing the centers of segments, a random “leaf” inclination drawn from a spherical distribution was assigned to each segment.

We simulated vertically homogeneous and vertically inhomogeneous forest structure (Figure 2) with LAI of 2, 4, or 6, for a total of six different sets of simulations. To compute relevant statistics, each set of simulations comprised 1000 realizations. For each simulation, 4000 rays were traced from the top of the canopy starting at locations drawn uniformly along the horizontal axis (0 and 200 m) and with angles drawn from a discrete uniform distribution in the interval $\pm 20^\circ$. Periodic conditions were applied to the boundaries. The positions where the rays intersect the leaves were recorded up through the tenth contact.

LAI and LAD profiles were estimated from these simulated lidar data using the algorithms given above. Bias and error in LAI were evaluated for varying number of returns used and for different numbers of pulses (250, 500, 1000, 2000, and 4000 pulses) for each set of simulations. Specifically, relative bias was defined as the mean difference between the estimated and true values divided by the true value; relative error was defined as the standard deviation of the estimates divided by the true value.

2.5. Empirical Case Study

We tested the model at an intensively studied 50 ha forest stand on Barro Colorado Island (BCI), Panama. Average precipitation is 2654 mm yr^{-1} , with a pronounced dry season between mid-December and end of

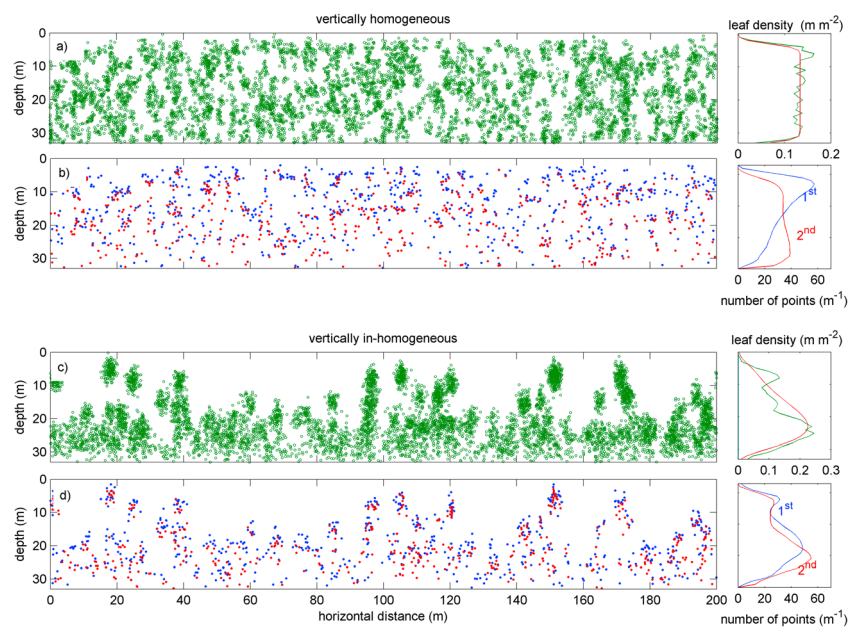


Figure 2. Examples of the two types of 2-D Shot Noise Cox Process simulations used to test the inversion algorithms: (a) a vertically homogenous simple cluster process and (c) a vertically in-homogenous complex cluster process, along with the (b and d) associated point clouds for first (blue) and second (red) returns of 1000 pulses. At right are the corresponding expected (red) and simulated (green) leaf density profiles and the frequency profiles of first and second returns. In both these cases, the leaf area index is 4 (parameter values in Appendix C).

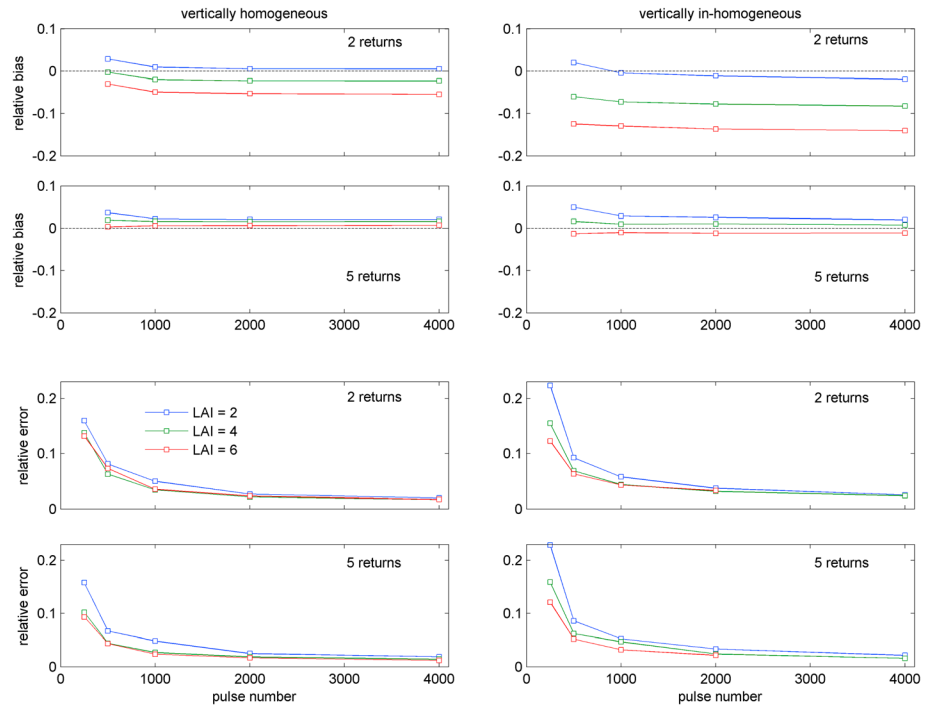


Figure 3. Influence of pulse number on the quality of LAI estimates for the two simulated forest types and three different LAI when using two or five returns. Relative bias is the mean difference between the estimated and true values divided by the true value; relative error is the standard deviation of the estimates divided by the true value.

April. Average air temperature is $\sim 26^{\circ}\text{C}$. The 50 ha plot is located on the top plateau of the island in old growth forest (> 400 years old), and the plot contains about 300 species of trees and 180 species of lianas, with diameter at breast height > 1 cm [Hubbell and Foster, 1983; Schnitzer et al., 2012]. In the dry season, 4–8% of canopy trees are deciduous at any given time [Condit et al., 2000].

The airborne data were collected in January 2012 using the Carnegie Airborne Observatory-Airborne Taxonomic Mapping System (CAO-AToMS) [Asner et al., 2012a, 2012b]. CAO-AToMS includes a dual laser, waveform lidar carried on a Dornier 228-202 aircraft. We collected AToMS data over the Barro Colorado 50 ha plot from an altitude of 1000 m above ground level, at an average flight speed of $55\text{--}60\text{ m s}^{-1}$ and a mapping swath of 0.6 km. The lidar has a beam divergence set to 0.56 mrad and was operated at 400 kHz.

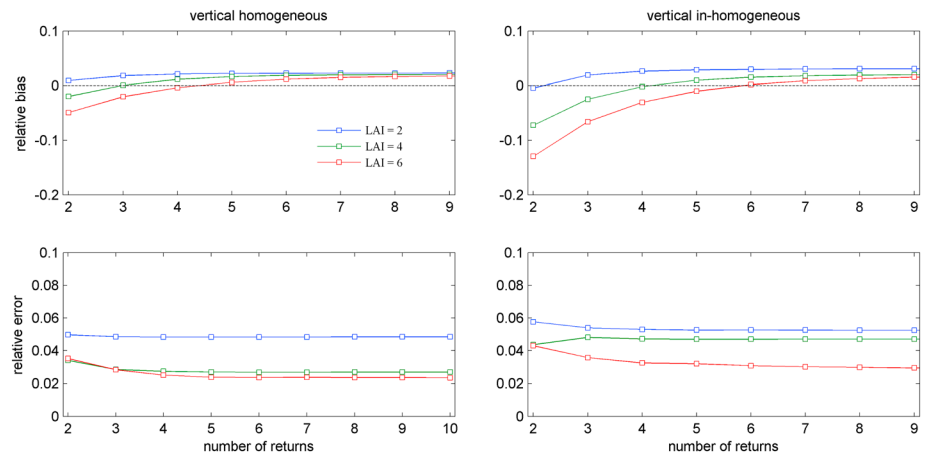


Figure 4. Influence of return number on LAI estimates for simulated 2-D canopies given data for 1000 pulses. Relative bias and error defined as in Figure 3.

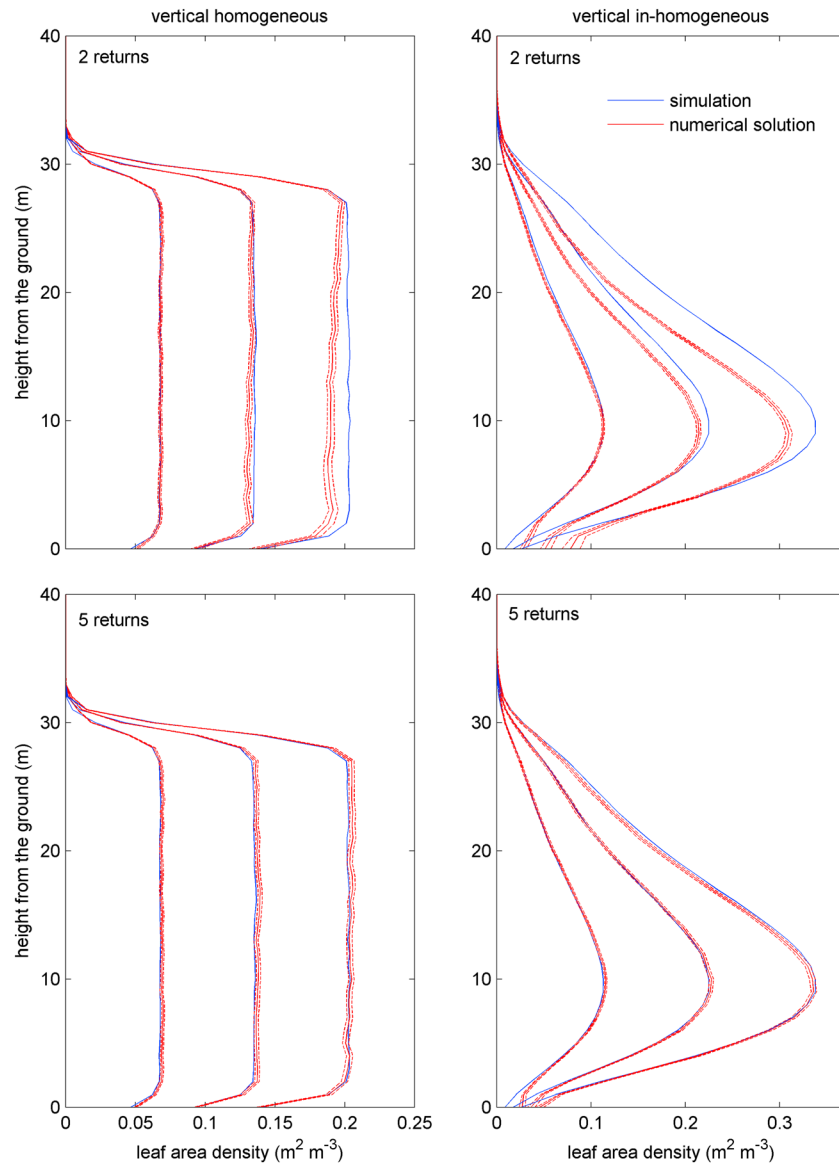


Figure 5. Sample ensemble of simulated (blue) and estimated (red) leaf area density profiles for the two sets of simulations (and LAI = 2, 4, and 6) when using (top row) two or (bottom row) five returns, with estimates based on 1000 pulses per simulation. Dashed lines represent the bootstrapped 95% confidence intervals around the mean estimated value.

Laser ranges from the lidar were combined with embedded high-resolution Global Positioning System-Inertial Measurement Unit data to determine the 3-D locations of laser returns, producing a “cloud” of lidar data. The lidar data cloud consists of a very large number of georeferenced point elevation estimates, where elevation is relative to a reference ellipsoid (WGS 1984). To estimate canopy height above ground, lidar data points were processed to identify which laser pulses penetrated the canopy volume and reached the ground surface. We used these points to interpolate a raster digital terrain model for the ground surface. This was achieved using a 10 m × 10 m kernel passed over each flight block; the lowest elevation estimate in each kernel was assumed to be ground. Subsequent points were evaluated by fitting a horizontal plane to each of the ground seed points. If the closest unclassified point was < 5.5° and < 1.5 m higher in elevation, it was classified as ground. This process was repeated until all points within the block were evaluated. Total number of points by return were 9,937,508 7,286,222 4,158,001 1,851,327, for first, second, third, and fourth return, respectively, for a total of 23,233,058 points, covering an area of approximately 50 ha.

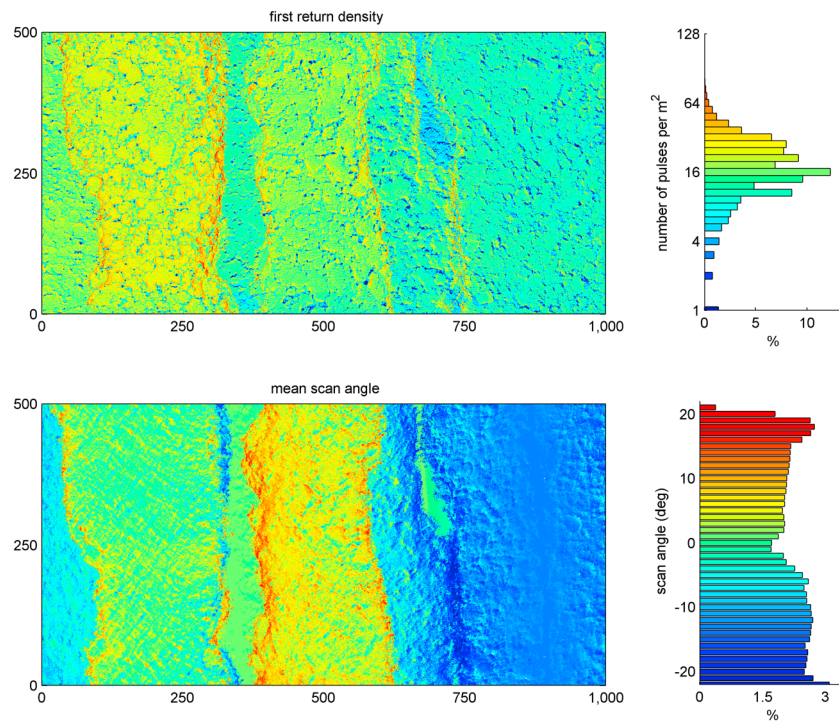


Figure 6. Nonuniform spatial sampling distribution of airborne lidar over the 50 ha plot on Barro Colorado Island, for first return density and mean scale angle at 1×1 m resolution (distance in meters). Frequency histograms for pulse density and all scan angles are also shown. Nonuniform sampling is inconsequential for estimating penetration functions if the sampling is uncorrelated with underlying forest structure, i.e., $I_0(\vec{\Omega}) = U_0(\vec{\Omega})$.

We evaluated the distribution of lidar sampling pulses and scan angles across the 50 ha plot. We then calculated the first- and second-order penetration functions and their variation with scan angle. Next, we applied the above algorithms in combination with several alternative assumptions about leaf angle to estimate LAD profiles using data for different numbers of returns. We used three theoretical leaf angle distributions described in *de Wit* [1965]—the spherical, erectophile, and planophile. In addition, we used a Campbell distribution [Campbell, 1986] parameterized with height-stratified empirical measurements from a previous study on BCI [Wirth *et al.*, 2001]. Finally, we divided the plot into 50×50 m quadrats and estimated LAI and LAD for each quadrat under the assumption of a spherical leaf angle distribution.

3. Results

3.1. Simulated Data Sets

For the vertically homogeneous forest structure scenario, relative bias in LAI was near zero and error was less than 5% for samples of 1000 or more pulses (Figure 3). For the vertically inhomogeneous forest structure scenario, relative bias was large for dense canopies and low return numbers (12% with two available returns) but decreased nearly to zero when five returns were available. Errors were somewhat larger than in the homogeneous case but decayed in a similar manner and were below 8% for samples of 1000 or more pulses. Biases were relatively insensitive to pulse number. The use of information from greater numbers of returns reduced the size of biases, especially in the vertically in-homogenous forest structure scenario, although there were decreasing gains from additional returns with little improvement beyond four to five returns (Figure 4). Errors were relatively insensitive to return number.

Leaf area density profiles were generally well described by the numerical solutions (Figure 5). For the homogeneous forest structure scenario, the largest deviations were at low heights in dense canopies with only two available returns. For the inhomogeneous forest structure scenario, there was underestimation even high in the canopy for dense canopies with only two available returns, but including more returns almost completely removed this bias.

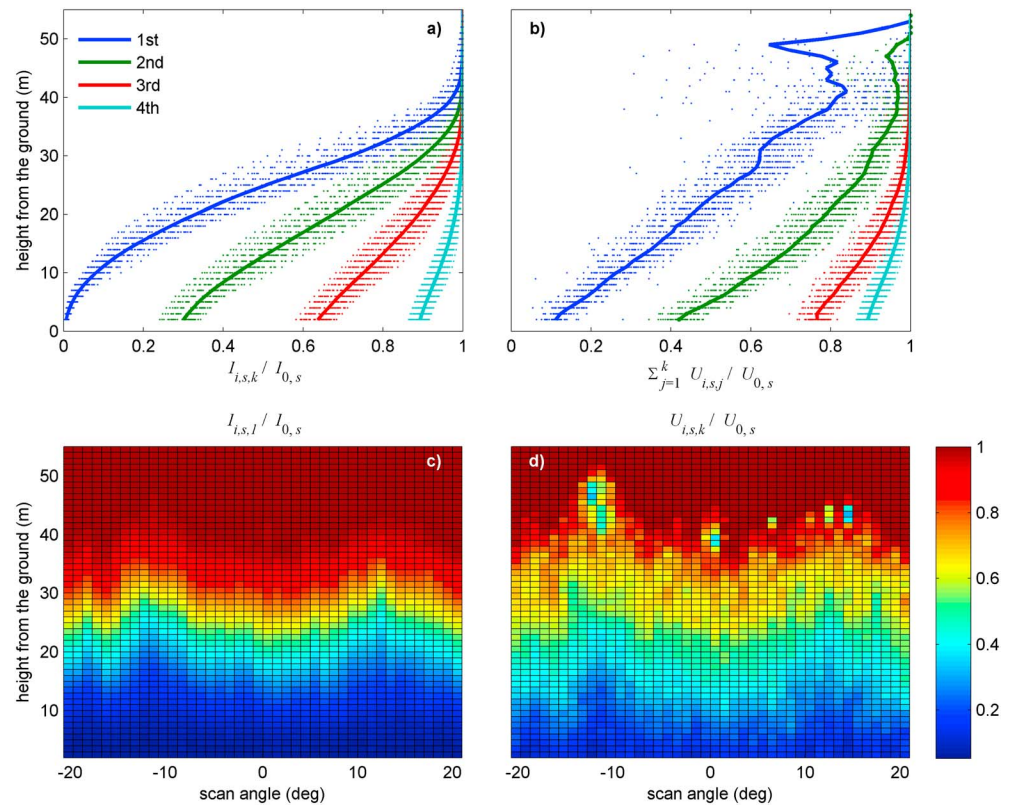


Figure 7. The mean (a) first-order penetration functions and (b) second-order penetration functions for different return number k . Bold lines are computed as means over all scan angles; dotted lines represent profiles for different scan angles. (c, d) The variation in the first return penetration functions with scan angle, that is, variation with scan angle in the proportion of beams which are not intercepted by leaves (gap fraction, Figure 7c) and in the proportion of the leaf area density which is directly exposed to radiation (sunlit leaves, Figure 7d).

3.2. Case Study of Airborne Lidar for a Tropical Forest

The airborne lidar sampling was not uniform over the 50 ha field plot. Pulses per square meter varied from 0 to 100 with mean 16. Scan angles spanned $\pm 21^\circ$. Large-scale heterogeneity was clearly related to flight lines (Figure 6). The distribution of number of first returns per square meter was approximately lognormal, while the distribution of scan angles was relatively uniform (Figure 6).

The median height from the ground at which the first pulses were intercepted was 25 m, and less than 1% of the first returns reached the ground surface (Figure 7a). At a height of 23 m, foliage had a 50% probability of being in direct sunlight and a 33% probability of being the second intercepted object (Figure 7b). These first- and second-order penetration functions showed some variation with scan angle (Figures 7c and 7d).

Estimated LAD profiles varied considerably depending upon the assumed leaf inclination angle distribution functions, as would be expected (Figures 8a and 8b). Estimates using just first and second returns showed higher leaf density at lower layers than those using more returns (Figures 8c and 8d).

Estimates of LAI for 50×50 m quadrats showed twofold spatial variation across the plot (Figure 9). Confidence limits on the mean distribution were nevertheless quite low (Figure 9).

4. Discussion

The new modeling approach presented here enables quantification of local spatial variation in leaf area density from small-footprint, multireturn lidar data, at spatial scales previously inaccessible using field studies. The new algorithms also provide a means to assess the sensitivity of such lidar to forest structural variation more generally. Our results suggest that utilizing the capability of multireturn, rather than one lidar data, reduces bias and errors in LAD estimation. Reasonably good LAD estimates (error SD < 10%) were obtained with 500 or more

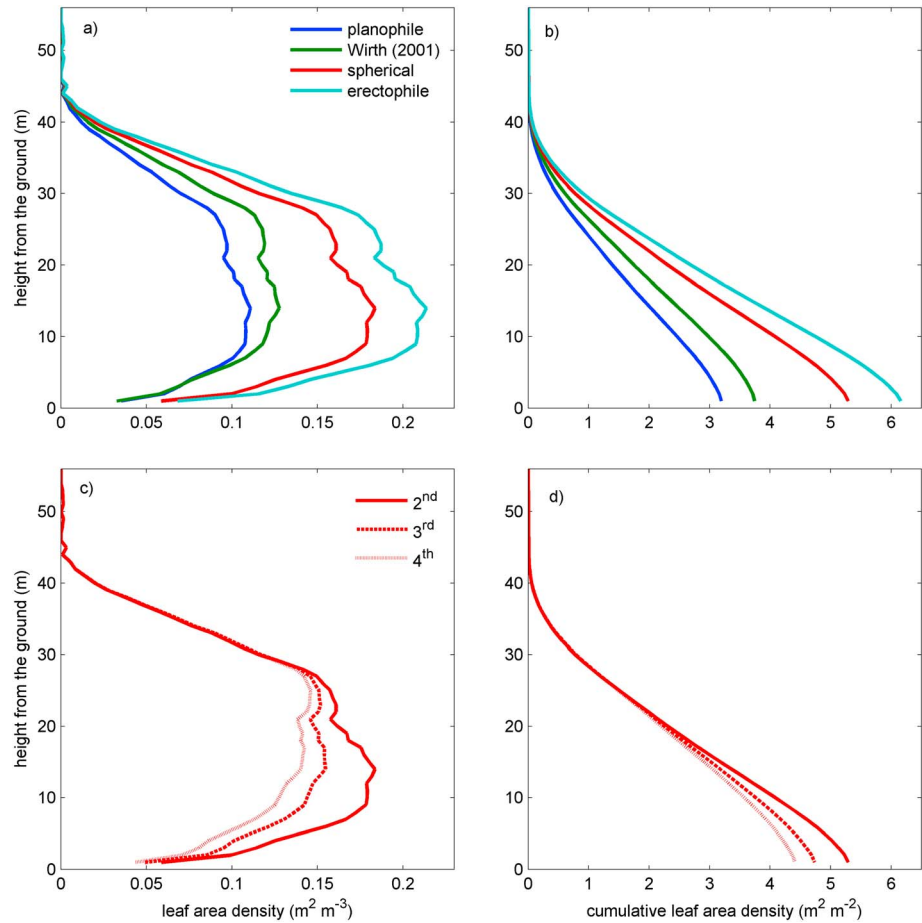


Figure 8. (a, b) Estimated leaf area density using different leaf inclination distribution functions. *Wirth et al.* [2001] used actual measurements of leaf inclination angles taken on Barro Colorado Island. (c, d) Estimated leaf area density for different maximum number of returns and spherical leaf angle distribution.

pulses in a simulated stand. Importantly, these simulations showed that the inversion algorithm was robust to forest structural complexity, although strong clumping and vertical inhomogeneity reduced performance, especially when beams have to pass through dense vegetation layers, as would be expected.

Applying our model to actual airborne lidar data revealed interesting forest structural properties that have not been assessed using field or other remote sensing techniques. On average, the first-order penetration functions, $I_{i,s,k}/I_{0,s}$ (the proportion of beams which are not intercepted by leaves), decayed monotonically and

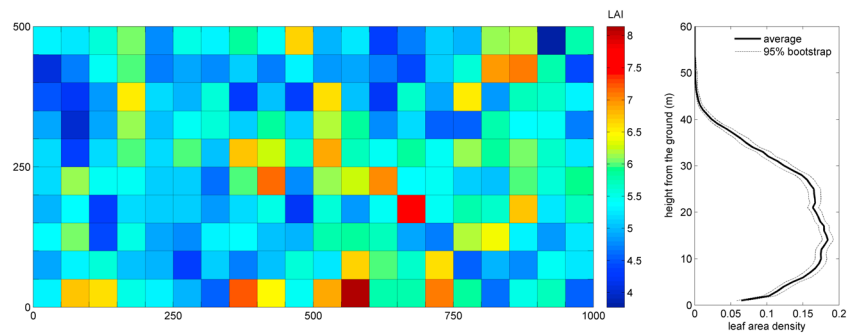


Figure 9. (left) Map of estimated LAI for 50 × 50 m quadrats and (right) the average of quadrat-level LAD profiles, with 95% confidence interval based on bootstrapping over 50 × 50 m quadrats. These estimates are based on the assumption of a spherical leaf angle distribution.

exponentially, as expected (Figure 7a). However, the second-order functions, $U_{i,s,k}/U_{0,s}$ (the proportion of LAD directly exposed to radiation), had a more complex pattern (Figure 7b). This vertical pattern can be attributed to emergent tree crowns, which generated strong clumping in the upper canopy, thereby reducing $U_{i,s,k}/U_{0,s}$ more rapidly than $I_{i,s,k}/I_{0,s}$. In the lower layers, $U_{i,s,k}/U_{0,s}$ increased in some cases and then decayed almost linearly and less rapidly than $I_{i,s,k}/I_{0,s}$, suggesting that the lower canopy tended to occupy gap (open) areas to minimize local-scale shade from upper layers.

LAI showed large variation within the 50 ha study area, with twofold variation even when computed at the fairly coarse spatial grain of 50×50 m (Figure 9). Such variation has potentially important implications for upscaling ecosystem functions from leaf to stand levels, because the function of the average is not equal to the average of the function for the relevant nonlinear processes [Rastetter *et al.*, 1992]. This suggests the need for further studies to better characterize and understand patterns of spatial variation in LAD. The observed spatial pattern of variation in LAI across the BCI 50 ha plot tracks topographic variation across the plot to some degree. Post hoc analyses revealed positive correlations between LAI and canopy height (results not shown). Future analyses should further explore predictors of LAD profiles within and across stands.

Penetration functions varied with scan angle, with a distinct and almost symmetric pattern (Figures 7c and 7d). More vertical scan angles allowed for more penetration of lidar beams. Penetration decreased at around $\pm 13^\circ$ but increased again for steeper angles. This result is inconsistent with radiative transport theory, which predicts a decrease in the penetration function with beam inclination, because forest optical thickness becomes larger and clumping effects become less important [Ross, 1981]. A possible explanation for this may be traced to the lidar footprint growing in cross section at higher scan angles, increasing the penetration capability of the beam. Differences among scan angles can also be attributed to spatial variability in the study area, as tall emergent trees are sporadically distributed and the distribution of scan angles varies systematically in space depending on position relative to the flight lines (Figure 6).

The assumed leaf inclination model constitutes a great source of uncertainty, requiring knowledge of the vertical variation of leaf inclination angle per species. Uncertainty in leaf inclination angle directly affects LAD estimates because of the proportionality between the effective (projected) LAD and (unprojected) LAD through the G-function (equation (1)). Wirth *et al.* [2001] used vertically stratified leaf inclination angle measurements and a simple light attenuation model to calculate LAI of around 5.1 for a small plot (0.21 ha) in another part of BCI during the dry season (and 5.4 in the wet season). Our estimation based on the leaf inclination measurement of Wirth *et al.* [2001] produced an LAI value of about 4.0 averaged over the entire 50 ha plot. However, assuming a spherical leaf inclination angle distribution with no vertical variation resulted in an LAI of ~ 5.2 . A recent study suggests that a spherical leaf inclination angle distribution is a poor model for temperate and boreal forests [Pisek *et al.*, 2013], and our leaf inclination angle measurements from eleven species on BCI suggest the same (Appendix D). The measured leaf angle distributions varied substantially among species and with height above ground (Tables D1 and D2). Furthermore, horizontal heterogeneity of mature tropical forests, as on BCI, can be quite large due to interspecific and environmental variation in leaf inclination. For example, leaves in gaps are generally more steeply inclined than leaves at the same height under closed canopies [Millen and Clendon, 1979; Falster and Westoby, 2003].

Although there is no direct measurement of LAI for BCI for the same area and time to use as a basis of comparison, our estimated LAI appeared to be on the lower end for type of moist old growth forest, at least in broad comparison to other tropical forests [Asner *et al.*, 2003]. The way the lidar waveform is acquired and processed may contribute to potential LAI underestimation due to missing target detection. A missing detection can happen when the signal fails to trigger a recording at the lidar receiver, or if the target is marginally hit, or if multiple targets are very close to one another along the path of the laser beam. The problem becomes increasingly acute for second and later returns because their signal-to-noise ratio is progressively smaller. Notably, including third and fourth returns significantly reduced LAI and LAD estimation (Figure 8), regardless of the leaf inclination angle model, which is inconsistent with simulations (Figures 4 and 5). Because the number of returns only marginally improves model performance, and third and fourth returns are prone to systematic errors, we recommend using only the first and second returns and applying a 10–15% correction for the bias observed in simulations (inhomogeneous simulation results for estimates based on two returns; Figures 3 and 4). Another issue for future consideration is the

sensitivity of the laser receivers relative to the power of the laser transmitters. These issues affect both the penetrability of the vegetation (power) and the ability to digitize the presence of foliar tissues at depth in the canopy. There is no one combination that is known to be optimal for small-footprint applications of lidar to forest canopies, but it does have an effect on estimates of canopy structure and derived products such as biomass [Asner and Mascaro, 2014]. Further methodological exploration should be directed to understand systematic errors caused by lidar sampling and processing, which may provide a way to correct biases in LAD estimation.

5. Conclusions

We developed a method to estimate the leaf area density and leaf area index of vegetation canopies using multireturn lidar data. Our method, based on radiative transport theory, can be easily applied to other lidar systems, both airborne and terrestrial, with the only difference being that the orientation of equations (4a) and (4b) needs to be adjusted. The proposed approach goes beyond the simple estimation of leaf area density by providing a meaningful counting method for multireturn lidar point clouds in the context of laser return number and scan angle. Of particular ecological interest is the normalized second-order function, $U(z, s, k)/U_0(s)$, basically the proportion of illuminated leaves at any depth in the canopy. It is related to the probability of a leaf to have one, two, or more leaves along the radiation path, and thus, it is closely related to light competition. Together, $I(z, s)/I_0(s)$ and $U(z, s)/U_0(s)$ are strong candidates for being good descriptors of forest spatial organization around limited light resources, although they are restricted to uncolloidal radiation fields. The algorithms developed here provide a solid basis for future studies of spatial variation in complex forest canopies, studies that promise insights into the organization of foliage and improvements in tools for upscaling from leaf to stand scales.

Appendix A: Stochastic Integral Radiative Transfer Equations for Penetration Functions Associated With a Multireturn Laser Beam

At each point in the canopy space, the intensity of the uncolloidal radiation associated with the k th return in the direction Ω equals the radiation at the top of the canopy plus an integral term that describes that radiation intercepted up to z . The intercepted term can be expressed as the difference between the radiation intercepted by the k th return and the radiation intercepted by the $(k - 1)$ th return, because this fraction of the radiation in reality passes through. So we can write

$$\begin{aligned} & |\mu|I^{(k)}\left(x, y, z, \vec{\Omega}\right) + a_L \int_0^z p\left(x + \frac{\Omega_x}{\Omega_z}z', y + \frac{\Omega_y}{\Omega_z}z', z'\right) G\left(z', \vec{\Omega}\right) I^{(k)}\left(x + \frac{\Omega_x}{\Omega_z}, y + \frac{\Omega_y}{\Omega_z}, z', \vec{\Omega}\right) dz' \\ & - a_L \int_0^z p\left(x + \frac{\Omega_x}{\Omega_z}, y + \frac{\Omega_y}{\Omega_z}z'\right) G\left(z', \vec{\Omega}\right) I^{(k-1)}\left(x, \frac{\Omega_x}{\Omega_z}y + \frac{\Omega_y}{\Omega_z}, z', \vec{\Omega}\right) dz' = |\mu|I_0\left(\vec{\Omega}\right) \end{aligned} \quad (\text{A1})$$

using the spatial average

$$|\mu|I^{(k)}\left(z, \vec{\Omega}\right) + \int_0^z u(z') G(z', \Omega) U^{(k)}\left(z', \vec{\Omega}\right) dz' = |\mu|I_0\left(\vec{\Omega}\right) \quad (\text{A2})$$

where

$$U^{(k)}\left(z, \vec{\Omega}\right) = \frac{\int p(x, y, z) \left(I^{(k)}(x, y, z, \Omega) - I^{(k-1)}(x, y, z, \Omega) \right) dx dy}{\int p(x, y, z) dx dy} \quad (\text{A3})$$

The second-order moment equation is derived multiplying equation (A1) by $p(x, y, z)$

$$\begin{aligned} & p(x, y, z) |\mu|I^{(k)}(x, y, z, \Omega) + a_L \int_0^z p(x, y, z) p(x, y, z') G(z', \Omega) I^{(k)}(x, y, z', \Omega) dz' \\ & - a_L \int_0^z p(x, y, z) p(x, y, z') G(z', \Omega) I^{(k-1)}(x, y, z', \Omega) dz' = a_L p(x, y, z) |\mu|I_0(\Omega) \end{aligned} \quad (\text{A4})$$

and taking the spatial average and dividing by $\int p(x, y, z) dx dy$:

$$|\mu| \sum_{j=1}^k U^{(j)}(z, \Omega) + \int_0^z g(z, z' \rightarrow \Omega) u(z') G(z', \Omega) U^{(k)}(z', \Omega) dz' = |\mu|U_0(z, \Omega) \quad (\text{A5})$$

In deriving (A5), we have used the following closure assumption:

$$\frac{a_L^2}{A} \int \rho(x, y, z) \rho(x, y, z') I^{(k)}(x, y, z', \Omega) dx dy \approx g(z, z') u(z') u(z) U^{(k)}(z', \Omega) \quad (\text{A6})$$

Note that in the case that the incident radiation field at the top of the canopy is uncorrelated with forest structure, $U_0(z, \Omega) = I_0(z, \Omega)$.

Appendix B: Estimation of Mean Intercepted Radiation per Unit of Leaf Area With Incomplete Return Numbers

In the case when all return numbers are available, the mean intercepted radiation per unit of leaf area associated with return number k can be estimated from the probability

$$\frac{U(z, s, k)}{U_0} = P(\rho = k | \zeta = z, \theta = s). \quad (\text{B1})$$

For $k = 1$, the above relationship expresses the conditional probability that given a leaf at depth z , there are no leaves above. In other words, it is the ratio between sunlit and shaded leaf area. When only points with return numbers up to k_{\max} are available, the estimated probability is related to the total probability by

$$P(\rho = k | \zeta = z, \theta = s, k \leq k_{\max}) = \frac{P(\rho = k | \zeta = z, \theta = s)}{P(\rho \leq k_{\max} | \zeta = z, \theta = s)} \quad (\text{B2})$$

Here $P(\rho \leq k_{\max} | \zeta = z, \theta = s)$ can be expressed as the sum of the k_{\max} normalized U functions:

$$P(\rho \leq k_{\max} | \zeta = z, \theta = s) = \sum_{i=1}^{k_{\max}} P(\rho = i | \zeta = z, \theta = s) = \sum_{i=1}^{k_{\max}} U(z, s, i) \quad (\text{B3})$$

Using equation (3b) in the main text, this term equals

$$\sum_{i=1}^{k_{\max}} U(z, s, i) = U_0(s) - |\cos(s)|^{-1} \int_0^z g(z, z', s) u(z') G(z', s) U(z', s, k_{\max}) dz' \quad (\text{B4})$$

If we assume for the purpose of deriving a correction factor that $g(z, z', s) \simeq 1$, we can substitute the integral in the left-hand side of the above equation using equation (3a)

$$\sum_{i=1}^{k_{\max}} U(z, s, i) \approx U_0(s) - I_0(s) + I(z, s, k_{\max}) \quad (\text{B5})$$

In the case $U_0(s) = I_0(s)$, i.e., radiation at the top of the canopy is independent on forest structure,

$\sum_{i=1}^{k_{\max}} U(z, s, i) = I(z, s, k_{\max})$ and it follows that

$$\frac{U(z, s, k)}{U_0} \approx P(\rho = k | \zeta = z, \theta = s, k \leq k_{\max}) \frac{I(z, s, k_{\max})}{I_0(s)} \quad (\text{B6})$$

If the probability to find a point with return number k_{\max} above depth z is negligible, i.e., $\frac{I(z, s, k_{\max})}{I_0(s)} \simeq 1$, the number of available returns is sufficient to represent the forest structure and the correction has no effect.

Appendix C: SNCP

A Shot Noise Cox Process is a random spatial process $Z(\mathbf{x})$ on a d -dimensional Euclidian space defining a set of points (offspring or leaves) conditional on another set of points (parents or crown centers)

Table D1. Species-Specific Statistics of Leaf Inclination Measurements Made Using a Leveled Digital Camera, Including Parameters of Best Fit Beta Functions

| Species Name | Count | Mean | SD | μ | ν |
|------------------------------|-------|-------|-------|-------|-------|
| <i>Desmopsis panamensis</i> | 261 | 26.27 | 14.02 | 2.19 | 5.32 |
| <i>Eugenia galalonensis</i> | 155 | 25.59 | 14.42 | 1.97 | 4.96 |
| <i>Eugenia oerstediana</i> | 462 | 27.51 | 14.99 | 2.03 | 4.61 |
| <i>Faramea occidentalis</i> | 285 | 22.28 | 12.98 | 1.97 | 5.98 |
| <i>Hybanthus prunifolius</i> | 78 | 15.60 | 10.80 | 1.55 | 7.40 |
| <i>Inga umbellifera</i> | 811 | 34.86 | 19.57 | 1.56 | 2.46 |
| <i>Luehea seemannii</i> | 345 | 30.75 | 15.49 | 2.25 | 4.34 |
| <i>Mauriri mytilloides</i> | 286 | 21.42 | 14.08 | 1.52 | 4.88 |
| <i>Swartzia simplex</i> | 192 | 21.48 | 14.58 | 1.41 | 4.51 |
| <i>Triplaris cumingiana</i> | 194 | 44.05 | 15.85 | 3.46 | 3.60 |

$\{p_j, j = 1, 2, \dots\}$ [Møller, 2003]. For simplicity we consider a bidimensional case, $\mathbf{x} = [x \ z]$, in the horizontal and vertical axis. We can express $Z(\mathbf{x})$ as

$$Z(\mathbf{x}) = \sum_j \gamma_j k(p_j, \sigma_j, \mathbf{x}) \tag{C1}$$

where $k(\mathbf{c}, \mathbf{x})$ is a kernel density function with dispersal parameter $\sigma = [\sigma_x \ \sigma_z]$ describing the distribution of leaves around the crown centers in the vertical and horizontal directions and γ is the expected number of leaves per crown. The crown centers are distributed as an inhomogeneous Poisson process with intensity function depending only on z . We consider two distributions: uniform and exponential

$$\zeta(z) = \begin{cases} \frac{\mu}{2h} & 0 < z \leq 2h \\ 0 & z > 2h \end{cases} \tag{C2}$$

$$\zeta(z) = \frac{\mu}{h} e^{-z/h}$$

where μ is the stem density and h the mean height of the crown centers. The dispersal parameters also depend on height from the ground according to allometric relationships $\sigma_x = az^b, \sigma_y = rz^b$, where r is an anisotropic parameter allowing for crown stretching/compressing in the vertical direction. γ also follows an allometric relationship $\gamma = cz^d$.

If ℓ_L is the size of one leaf, the leaf area index (LAI) can be computed as

$$LAI = \ell_L \int \zeta(z) \gamma(z) dz \tag{C3}$$

The first- and second-order intensity of a SNCP can be expressed as [Møller, 2003; Henrys and Brown, 2009]

Table D2. Statistics of Leaf Inclination Measurements Made Using a Leveled Digital Camera, Including Parameters of Best Fit Beta Functions, By Height Class

| Height (m) | Count | Mean | SD | μ | ν |
|------------|-------|-------|-------|-------|-------|
| 0–2 | 263 | 22.49 | 13.27 | 1.90 | 5.72 |
| 2–4 | 447 | 23.99 | 14.68 | 1.69 | 4.65 |
| 4–6 | 562 | 22.52 | 13.66 | 1.79 | 5.36 |
| 6–8 | 264 | 21.71 | 14.18 | 1.54 | 4.84 |
| 8–10 | 188 | 23.23 | 14.24 | 1.72 | 4.93 |
| 10–12 | 160 | 26.68 | 14.21 | 2.18 | 5.18 |
| 12–14 | 106 | 28.62 | 14.57 | 2.31 | 4.96 |
| 14–16 | 238 | 33.23 | 15.68 | 2.47 | 4.21 |
| 16–18 | 226 | 39.56 | 15.33 | 3.29 | 4.20 |
| 18–20 | 255 | 41.11 | 16.94 | 2.74 | 3.26 |
| 20–22 | 184 | 38.94 | 20.61 | 1.59 | 2.09 |
| 22–24 | 176 | 43.08 | 20.38 | 1.85 | 2.02 |

$$\lambda(\mathbf{x}) = \int \gamma(p) k(p, \sigma(p), \mathbf{x}) d\zeta(p)$$

$$\lambda_2(\mathbf{x}_1, \mathbf{x}_2) = \int \gamma(c)^2 k(p, \sigma(p), \mathbf{x}_1) k(p, \sigma(p), \mathbf{x}_2) d\zeta(c) \quad (C4)$$

Along the vertical direction, leaf area density $u(z)$ and pair correlation function $g(z_1, z_2, 0) = 1 + \frac{\lambda_2(z_1, z_2)}{\lambda(z_1)\lambda(z_2)}$ can be computed numerically using a Gaussian kernel $G(z)$ from the following integrals:

$$u(z) = \ell \int \gamma(z') G\left(\frac{z - z'}{\sigma_V(z')}\right) \zeta(z') dz'$$

$$g(z_1, z_2, 0) = 1 + \frac{\ell^2 \int \gamma(z')^2 \frac{1}{\sqrt{8\pi\sigma_H(z')^2}} G\left(\frac{z_1 - z'}{\sigma_V(z')}\right) G\left(\frac{z_2 - z'}{\sigma_V(z')}\right) \zeta(z') dz'}{u(z_1)u(z_2)} \quad (C5)$$

Appendix D: Leaf Angle Distribution

In March 2013, leaf inclination angles of 10 BCI tree representative species on BCI were measured at 2 m height intervals using digital photography following the approach first introduced by *Ryu et al.* [2010] and evaluated by *Pisek et al.* [2011]. For each species we calculated mean and standard deviation of the leaf angle distribution and fitted a beta distribution.

Acknowledgments

This work was supported by Smithsonian Institution Global Earth Observatory (SIGEO) and Carnegie Airborne Observatory (CAO). CAO is made possible by the Gordon and Betty Moore Foundation, the John D. and Catherine T. MacArthur Foundation, W.M. Keck Foundation, the Margaret A. Cargill Foundation, Grantham Foundation for the Protection of the Environment, Mary Anne Nyburg Baker and G. Leonard Baker Jr., and William R. Hearst III. Anyone wishing collaborate on use of the lidar data analyzed here should contact Gregory Asner (gpa@stanford.edu) with the request.

References

- Asner, G., J. Scurlock, and J. Hicke (2003), Global synthesis of leaf area index observations: Implications for ecological and remote sensing studies, *Global Ecol. Biogeogr.*, *12*, 191–205.
- Asner, G. P., and J. Mascaro (2014), Mapping tropical forest carbon: Calibrating plot estimates to a simple LiDAR metric, *Remote Sens. Environ.*, *140*, 624–614.
- Asner, G. P., et al. (2010), High-resolution forest carbon stocks and emissions in the Amazon, *Proc. Natl. Acad. Sci. U.S.A.*, *107*(38), 16,738–16,742, doi:10.1073/pnas.1004875107.
- Asner, G. P., D. E. Knapp, J. Boardman, R. O. Green, T. Kennedy-Bowdoin, M. Eastwood, R. E. Martin, C. Anderson, and C. B. Field (2012a), Carnegie Airborne Observatory-2: Increasing science data dimensionality via high-fidelity multi-sensor fusion, *Remote Sens. Environ.*, *124*, 454–465.
- Asner, G. P., et al. (2012b), High-resolution mapping of forest carbon stocks in the Colombian Amazon, *Biogeosciences*, *9*(7), 2683–2696, doi:10.5194/bg-9-2683-2012.
- Béland, M., J.-L. Widlowski, and R. A. Fournier (2014), A model for deriving voxel-level tree leaf area density estimates from ground-based LiDAR, *Environ. Modell. Softw.*, *51*, 184–189, doi:10.1016/j.envsoft.2013.09.034.
- Bréda, N. J. J. (2003), Ground-based measurements of leaf area index: A review of methods, instruments and current controversies, *J. Exp. Bot.*, *54*(392), 2403–2417, doi:10.1093/jxb/erg263.
- Campbell, G. (1986), Extinction coefficients for radiation in plant canopies calculated using an ellipsoidal inclination angle distribution, *Agric. For. Meteorol.*, *36*, 317–321.
- Chen, J. M., P. M. Rich, S. T. Gower, J. M. Norman, and S. Plummer (1997), Leaf area index of boreal forests: Theory, techniques, and measurements, *J. Geophys. Res.*, *102*(D24), 29,429–29,443, doi:10.1029/97JD01107.
- Clark, D., P. Olivas, S. Oberbauer, D. Clack, and M. Ryan (2008), First direct landscape-scale measurement of tropical rain forest Leaf Area Index, a key driver of global primary productivity, *Ecol. Lett.*, *11*(2), 163–172, doi:10.1111/j.1461-0248.2007.01134.x.
- Condit, R., K. Watts, S. Bohlman, R. Pérez, R. Robin, and S. Hubbell (2000), Quantifying the deciduousness of tropical forest canopies under varying climates, *J. Veg. Sci.*, *11*(5), 649–658.
- Daley, D., and D. Vere-Jones (2003), An introduction to the theory of point processes, in *Volume I: Elementary Theory and Methods*, 2nd ed., Springer, New York.
- Detto, M., H. C. Muller-Landau, J. Mascaro, and G. P. Asner (2013), Hydrological networks and associated topographic variation as templates for the spatial organization of tropical forest vegetation, *PLoS One*, *8*(10), e76296, doi:10.1371/journal.pone.0076296.
- De Wit, C. T. (1965), Photosynthesis of leaf canopies, Agricultural Research, Rep. no. 663. [Available at <http://edepot.wur.nl/187115>, Accessed 22 July 2014.]
- Falster, D. S., and M. Westoby (2003), Leaf size and angle vary widely across species: What consequences for light interception?, *New Phytol.*, *158*(3), 509–525, doi:10.1046/j.1469-8137.2003.00765.x.
- Flaspohler, D. J., C. P. Giardina, G. P. Asner, P. Hart, J. Price, C. K. Lyons, and X. Castaneda (2010), Long-term effects of fragmentation and fragment properties on bird species richness in Hawaiian forests, *Biol. Conserv.*, *143*(2), 280–288, doi:10.1016/j.biocon.2009.10.009.
- Gamon, J., C. Field, M. Goulden, K. Griffin, and A. Hartley (1995), Relationships between NDVI, canopy structure, and photosynthesis in three Californian vegetation types, *Ecol. Appl.*, *5*(1), 28–41.
- Hardiman, B. S., G. Bohrer, C. M. Gough, C. S. Vogel, and P. S. Curtis (2011), The role of canopy structural complexity in wood net primary production of a maturing northern deciduous forest, *Ecology*, *92*(9), 1818–1827.
- Henry, P. A., and P. E. Brown (2009), Inference for clustered inhomogeneous spatial point processes, *Biometrics*, *65*(2), 423–430, doi:10.1111/j.1541-0420.2008.01070.x.

- Hosoi, F., Y. Nakai, and K. Omasa (2013), Voxel tree modeling for estimating leaf area density and woody material volume using 3-D LIDAR data, *ISPRS Ann. Photogramm. Remote Sens. Spat. Inf. Sci., II-5/W2*, 115–120, doi:10.5194/isprsannals-II-5-W2-115-2013.
- Hubbell, S., and R. Foster (1983), Diversity of canopy trees in a neotropical forest and implications for conservation, in *Tropical Rain Forest: Ecology and Management*, edited by S. Sutton, T. Whitmore, and A. Chadwick, pp. 25–41, Blackwell Scientific Publications, Oxford.
- Jarvis, P. G., and K. G. McNaughton (1986), Stomatal control of transpiration: Scaling up from leaf to region, *Adv. Ecol. Res.*, 15(C), 1–49.
- Kotchenova, S. Y. (2003), Modeling lidar waveforms with time-dependent stochastic radiative transfer theory for remote estimations of forest structure, *J. Geophys. Res.*, 108(D15), 4484, doi:10.1029/2002JD003288.
- Lefsky, M. A., W. B. Cohen, G. G. Parker, and D. J. Harding (2002), Lidar remote sensing for ecosystem studies, *BioScience*, 52(1), 19, doi:10.1641/0006-3568(2002)052[0019:LRSFES]2.0.CO;2.
- Mascaro, J., G. P. Asner, H. C. Muller-Landau, M. van Breugel, J. Hall, and K. Dahlin (2011), Controls over aboveground forest carbon density on Barro Colorado Island, Panama, *Biogeosciences*, 8(6), 1615–1629, doi:10.5194/bg-8-1615-2011.
- McMahon, S. M., D. P. Bebbler, N. Butt, M. Crockatt, K. Kirby, G. G. Parker, T. Riutta, and E. M. Slade (2015), Ground based LiDAR demonstrates the legacy of management history to canopy structure and composition across a fragmented temperate woodland, *For. Ecol. Manage.*, 335, 255–260, doi:10.1016/j.foreco.2014.08.039.
- Meyer, V., S. S. Saatchi, J. Chave, J. W. Dalling, S. Bohlman, G. A. Fricker, C. Robinson, M. Neumann, and S. Hubbell (2013), Detecting tropical forest biomass dynamics from repeated airborne lidar measurements, *Biogeosciences*, 10(8), 5421–5438, doi:10.5194/bg-10-5421-2013.
- Millen, G. M., and J. M. Clendon (1979), Leaf angle: An adaptive feature of sun and shade leaves, *Bot. Gaz.*, 140(4), 437–442.
- Moller, J. (2003), Shot noise Cox processes, *Adv. Appl. Probab.*, 35(3), 614–640.
- Ni-Meister, W., D. Jupp, and R. Dubayah (2001), Modeling lidar waveforms in heterogeneous and discrete canopies, *IEEE Trans. Geosci. Remote Sens.*, 39(9), 1943–1958.
- Olivas, P. C., S. F. Oberbauer, D. B. Clark, D. A. Clark, M. G. Ryan, J. J. O'Brien, and H. Ordoñez (2013), Comparison of direct and indirect methods for assessing leaf area index across a tropical rain forest landscape, *Agric. For. Meteorol.*, 177, 110–116, doi:10.1016/j.agrformet.2013.04.010.
- Parker, G., D. Harding, and M. Berger (2004), A portable LIDAR system for rapid determination of forest canopy structure, *J. Appl. Ecol.*, 41, 755–767.
- Pisek, J., Y. Ryu, and K. Alikas (2011), Estimating leaf inclination and G-Function from leveled digital camera photography in Broadleaf Canopies, *Trees*, 25(5), 919–924, doi:10.1007/s00468-011-0566-6.
- Pisek, J., O. Sonnentag, A. D. Richardson, and M. Möttus (2013), Is the spherical leaf inclination angle distribution a valid assumption for temperate and boreal broadleaf tree species?, *Agric. For. Meteorol.*, 169, 186–194, doi:10.1016/j.agrformet.2012.10.011.
- Rastetter, E. B., A. W. King, B. J. Cosby, G. M. Hornberger, R. V. O. Neill, and J. E. Hobbie (1992), Aggregating fine-scale ecological knowledge to model coarser-scale attributes of ecosystems, *Ecol. Appl.*, 2(1), 55–70.
- Richardson, J. J., L. M. Moskal, and S.-H. Kim (2009), Modeling approaches to estimate effective leaf area index from aerial discrete-return LIDAR, *Agric. For. Meteorol.*, 149(6–7), 1152–1160, doi:10.1016/j.agrformet.2009.02.007.
- Ross, J. (1981), *The Radiation Regime and Architecture of Plant Stands*, Dr W Junk Publisher, The Hague.
- Ryu, Y., O. Sonnentag, T. Nilson, R. Vargas, H. Kobayashi, R. Wenk, and D. D. Baldocchi (2010), How to quantify tree leaf area index in an open Savanna Ecosystem: A multi-instrument and multi-model approach, *Agric. For. Meteorol.*, 150, 63–76.
- Schnitzer, S., et al. (2012), Liana abundance, diversity, and distribution on Barro Colorado Island, Panama, *PLoS One*, 7(12), e52114, doi:10.1371/journal.pone.0052114.
- Shabanov, N. V., Y. Knyazikhin, F. Baret, and R. B. Myneni (2000), Stochastic modeling of radiation regime in discontinuous vegetation canopies, *Remote Sens. Environ.*, 74(1), 125–144, doi:10.1016/S0034-4257(00)00128-0.
- Shugart, H. H., S. Saatchi, and F. G. Hall (2010), Importance of structure and its measurement in quantifying function of forest ecosystems, *J. Geophys. Res.*, 115, G00E13, doi:10.1029/2009JG000993.
- Stark, S. C., et al. (2012), Amazon forest carbon dynamics predicted by profiles of canopy leaf area and light environment, *Ecol. Lett.*, 15(12), 1406–1414, doi:10.1111/j.1461-0248.2012.01864.x.
- Titov, G. (1990), Statistical description of radiation transfer in clouds, *J. Atmos. Sci.*, 47(1), 24–38.
- Wagner, W., A. Ullrich, T. Melzer, C. Briese, and K. Kraus (2004), From single-pulse to full-waveform airborne laser scanners: Potential and practical challenges, *Int. Arch. Photogramm. Remote Sens.*, 35, 201–2016.
- Wagner, W., A. Roncat, T. Melzer, and A. Ullrich (2007), Waveform analysis techniques in airborne laser scanning, *Int. Arch. Photogramm. Remote Sens.*, 36, 413–418.
- Wiegand, T., I. Martínez, and A. Huth (2009), Recruitment in tropical tree species: Revealing complex spatial patterns, *Am. Nat.*, 174(4), E106–E140, doi:10.1086/605368.
- Wirth, R., B. Weber, and R. J. Ryel (2001), Spatial and temporal variability of canopy structure in a tropical moist forest, *Acta Oecol.*, 22(5-6), 235–244, doi:10.1016/S1146-609X(01)01123-7.
- Wu, J., Y. Liu, and D. E. Jelinski (2000), Effects of leaf area profiles and canopy stratification on simulated energy fluxes: The problem of vertical spatial scale, *Ecol. Modell.*, 134(2–3), 283–297, doi:10.1016/S0304-3800(00)00353-7.
- Zhao, K., and S. Popescu (2009), Lidar-based mapping of leaf area index and its use for validating GLOBCARBON satellite LAI product in a temperate forest of the southern USA, *Remote Sens. Environ.*, 113(8), 1628–1645, doi:10.1016/j.rse.2009.03.006.